Revista GEOCIÊNCIAS

unesp

ISSN: 1980-900X (online)

PETROLOGY, GEOCHEMISTRY AND MONAZITE U-Th-Pb AGES OF WEST ÁGUA RASA PALEOPROTEROZOIC POST-COLLISIONAL METAGRANITES FROM SOUTHERN SÃO FRANCISCO CRATON – BRAZIL

PETROLOGIA, GEOQUÍMICA E IDADES U-Th-Pb DE MONAZITAS DOS METAGRANITOS PALEOPROTEROZÓICOS PÓS-COLISIONAIS ÁGUA RASA OESTE DO CRÁTON DO SÃO FRANCISCO MERIDIONAL

Luiza Carneiro de REZENDE, Alexandre de Oliveira CHAVES

Universidade Federal de Minas Gerais. Instituto de Geociências. Avenida Presidente Antônio Carlos, 6627 - Pampulha, Belo Horizonte – MG. E-mails: luizacrez@gmail.com; alochaves@yahoo.com.br

ABSTRACT - During the transition of Rhyacian to Orosirian periods a collision between the Archean Divinópolis and Campo Belo metamorphic complexes occurred in southern São Francisco Craton (SFC) followed by the collapse of the orogen. In the same region, the Statherian period is marked by a huge intraplate magmatic event that is represented in the area by the Para de Minas dyke swarm. Peraluminous granitoid occurrences are reported in the region of Formiga and Itapecerica (Minas Gerais – Brazil), surrounding high metamorphic grade khondalitic paragneisses and banded iron formations. To contribute to the understanding of the tectonic context of the southern SFC during the Paleoproterozoic era, these granitic rocks are studied based on petrographic, geochemical, and monazite U-Th-Pb geochronological analyzes. They were characterized as S-type (metasedimentary origin) peraluminous metamonzogranites, with crustal geochemical signature, and genesis related to anatexis in syn- to post-collisional environment. The geochronological results yielded two groups of Orosirian (~1.90 Ga) and Statherian (~1.78 Ga) ages. These results are related, respectively, to the collapse of the Rhyacian-Orosirian orogen and to the regional warming, associated with the Avanavero-Xiong'er LIP that is represented in the area by the Pará de Minas dyke swarm.
Keywords: Anatexis. Monazite U-Th-Pb geochronology. Paleoproterozoic. São Francisco Craton. LIP.

RESUMO - Durante a transição entre os períodos Riaciano e Orosiriano, no sul do Cráton do São Francisco (CSF), ocorreu uma colisão entre os complexos metamórficos arqueanos Divinópolis e Campo Belo, seguida do colapso orogênico. Na mesma região, o período Estateriano é marcado por um enorme evento magmático intraplaca que é representado na área pelo enxame de diques Para de Minas. Ocorrências de granitóides peraluminosos são relatadas na região de Formiga e Itapecerica (Minas Gerais - Brasil), circundando paragnaisses kondalíticos de alto grau metamórfico e formações ferríferas bandadas. Para contribuir com a compreensão do contexto tectônico do sul do CSF durante a era Paleoproterozóica, essas rochas graníticas foram estudadas com base na petrografia, geoquímica e geocronológica U-Th-Pb em monazita. As amostras foram caracterizadas como metamonzogranitos peraluminosos do tipo S (origem metassedimentar), com assinatura geoquímica crustal, e gênese relacionada à anatexia em ambiente sin- a pós-colisional. Os resultados geocronológicos produziram dois grupos de idades: Orosiriana (~1,90 Ga) e Estateriana (~1,78 Ga). Esses resultados estão relacionados, respectivamente, ao colapso do orógeno Riacian-Orosiriano e ao aquecimento regional, associado à LIP Avanavero-Xiong'er que é representado na área pelo enxame de diques Pará de Minas.
Palavras-Chave: Anatexia. Geocronologia U-Th-Pb em monazita. Paleoproterozoico. Cráton do São Francisco. LIP.

INTRODUCTION

Granite is an igneous coarse-grained rock, composed mostly by quartz, alkali-feldspar, plagioclase and mica (Read, 1943). Granitic rocks are the most abundant igneous rocks on the Earth's continental crust and are found in various tectonic settings. They can be formed in orogenic and continental collision zones, anorogenic intraplate settings, mid-ocean ridges, ophiolite complexes, and also as plutons (Edmonds & Gill, 2010). An interesting origin granitic magma can present is by anatexis.

Anatexis is the process in which magma is formed by partial melting of crustal rocks (Ashworth, 1985). It plays an important role of active defor-

mation and emplacement of crustal granites (Brown & Solar, 1998), especially when it comes from sediments (Harris et al., 2000). Different geochemical signature can evidence the supracrustal origin from granites (Frost et al., 2001; Whalen et al., 1987; Chappell & White, 2001; Laurent et al., 2014) and can relate to different tectonic setting (Batchelor & Bowden, 1985; Pearce, 1996).

Accordantly to Miranda et al. (2020) there are occurrences of metagranites with sedimentary origin, named Água Rasa, in the southern portion of the São Francisco Craton (SFC) (Figure 1B) in the region of Itapecerica (Minas Gerais – Brazil) (Figure 1B). They analyzed those rocks and, with geochemical and geochronological data, associated their origin to the anatexis of supracrustal sequences, process related to the Rhyacian-Orosirian event reported in this area (Chaves et al., 2015; Carvalho et al., 2017; Miranda et al., 2020; Chaves, 2021).

Based on gamma spectrometric image (Figure 1C), metagranite samples that occurs between Formiga and Itapecerica (Figure 1A) were studied in this paper. The study aims to characterize the nature, origin, and age of what was called West Água Rasa Granite, using petrography, geochemistry, and monazite U-Th-Pb geochronology. The results are used to corroborate to the understanding of the Paleoproterozoic tectonic context in the southern SFC.

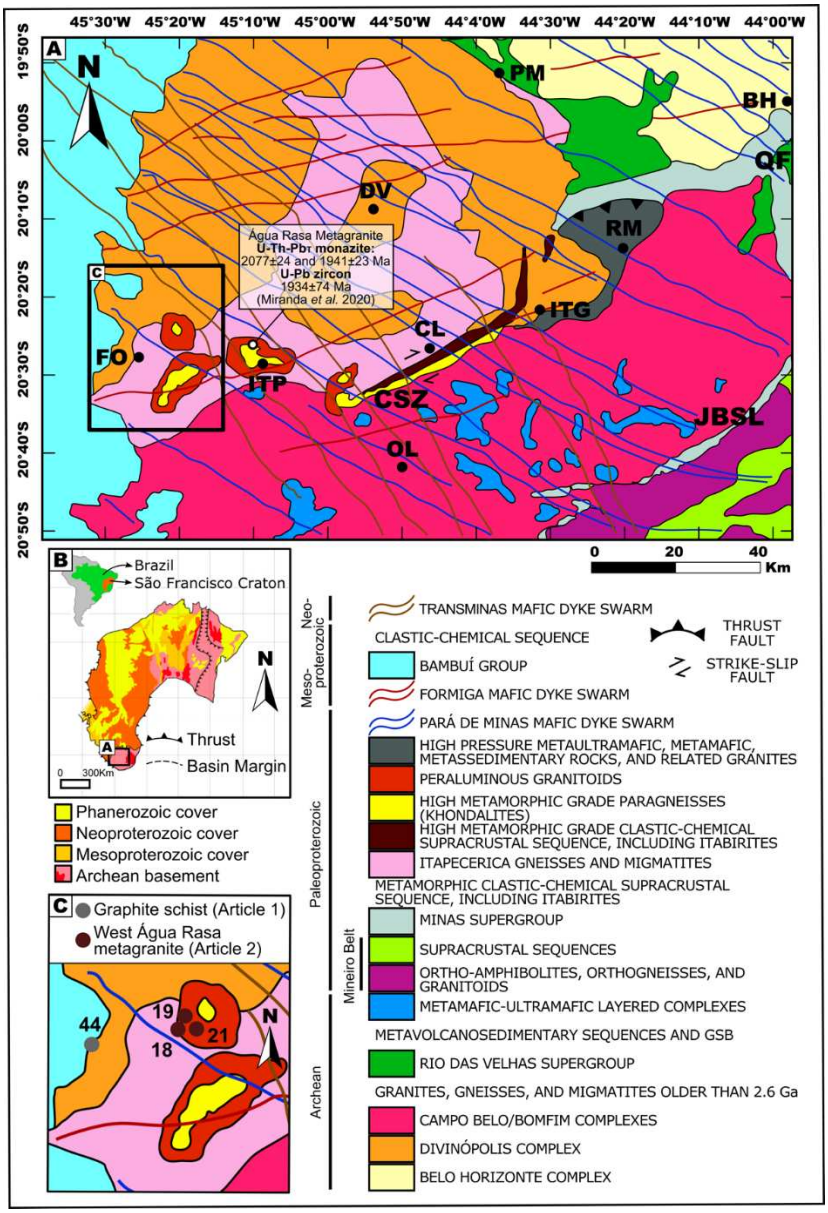

Figure 1 - (A) Geological map of the Southern São Francisco Craton, interpreted from geophysics, with the area of study highlighted. CSZ – Cláudio Shear Zone, JBSL – Jeceaba-Bom Sucesso Lineament, QF – Quadrilátero Ferrífero, Cities: BH – Belo Horizonte, CL – Cláudio, DV – Divinópolis, FO – Formiga, ITG – Itaguara, ITP – Itapecerica, OL – Oliveira, PM – Pará de Minas, RM – Rio Manso. Modified after Chaves & Porcher (2020). (B) São Francisco Craton simplified map, with its Southern region highlighted. Modified after Drummond et al. (2015). (C) K-Th-U ternary gamma spectrometric image of the area of study with the samples collecting sites highlighted (CPRM-CODEMIG, 2014).

GEOLOGICAL SETTING

The southern part of the SFC (Figure 1B) is composed by an Archean crust (3.5 – 2.6 Ga) that is constituted mostly by granite-gneisses rocks (Farina et al., 2015; Teixeira et al., 2017) and rocks from Rio das Velhas Supergroup, that are greenstone belts formed by mafic-ultramafic rocks, intermediate-felsic volcanic and volcanoclastic rocks (Noce et al., 1998) and terrigenous sediments (Dorr, 1969; Baltazar & Zucchetti, 2007).

Above the basement, that comprehends Campo Belo, Divinópolis, Bonfim and Belo Horizonte metamorphic complexes (Machado Filho et al., 1983; Teixeira et al., 1996), occurs the supracrustal sequence that includes the Minas Supergroup and Bambuí Group. The first unit is formed by Paleoproterozoic clastic-chemical metasedimentary rocks, with minimum deposition around 2.0 Ga, and also the typical banded iron formations from the Quadrilátero Ferrífero (Machado et al., 1996; Moreira et al., 2016). Neoproterozoic pelitic-carbonate sedimentary rocks from Bambuí Group (Alkmim & Martins-Neto, 2001) cover the basement. All the southern SFC is crosscuted by mafic dykes (Chaves et al., 2013). An orogeny that occurred between the Rhyacian and Orosirian resulted in extensive reworking of the margins of the southern portion of the SFC (Noce et al., 2007) and is also responsible for the formation of the Mineiro Belt (Noce et al., 1998; Ávila et al., 2014; Teixeira et al., 2015). The existence of a Paleoproterozoic event in the Itapecerica region was firstly suggested by Chaves et al. (2015) based on chemical ages found in monazites from sillimanite-cordierite-garnet-biotite gneiss (graphite-rich khondalitic rocks) and then confirmed by Carvalho et al. (2017) with isotopic ages of 2.05-2.03 Ga (U-Pb) found in zircons from the interior of the basement. Miranda et al. (2020) studied Água Rasa metagranites (Figure 1A), rocks that occur around the occurrences of khondalite, in which isotopic ages of zircons yield upper intercept of 1934 ± 74 Ma and chemical ages of monazites yield mean ages of 1941 ± 23 Ma and 2077 ± 24 Ma.

The area of the study (Figure 1A) is located in Formiga region, close to Itapecerica. This area was described by Carneiro & Barbosa (2008) as containing Mesoproterozoic gneisses, metagranitoids, amphibolites, mafic, metaultramafic and metacharnocktic rocks, recrystallized under the conditions of amphibolite to granulite facies (Fernandes & Carneiro, 2000). Elliptical anomalies, visible on gamma-ray ternary K-Th-U map (Figure 1C), are resulted of the presence of khondalitic graphite-rich rocks and banded iron formations and are contoured by metagranites known as Água Rasa, which are the object of study of this research.

METHODS

The samples were collected from three different sites (Figure 1C) located northeast from Formiga (20º24'45.4"S, 45º22'30.9"W). Six samples (18A, 18B, 19A, 19B, 21A and 21B) of West Água Rasa metagranite were used for petrographic and geochemical investigations and sample 21A was also used for geochronological analyses.

Petrography

Six thin sections were prepared and examined under transmitted and reflected light microscopy at the CPMTC-UFMG (Professor Manoel Teixeira da Costa Research Centre of the Federal University of Minas Gerais).

Whole rock geochemistry

Six granite samples have been sent to whole rock geochemistry analyses in SGS-Geosol Laboratory.

They were milled in tungsten mill, melted with lithium metaborate and diluted by nitric digestion. ICP-OES (Optical Emission Spectrometry with Inductively Coupled Plasma was used to analyze major elements and five trace elements (Ba, Sr, Zn, Zr and V), with detection limits of 0.01% and between 5 and 10 ppm, respectively.

Other trace elements and rare earth elements were analyzed by ICP-MS (Inductively Coupled Plasma Mass Spectrometry) with detection limits ranging from 0.02 to 5 ppm. The loss on ignition (LOI) was made by mass difference after heating at 1000ºC. The geochemical data was examined using Microsoft Excel supplement Geoplot (Zhou & Li, 2006).

Monazite mineral chemistry and U-Th-Pb_T geochronology

Three different monazite grains from a granite sample were analyzed in polished thin section using a JXA-8900 JEOL electron microprobe (EMP), at Microanalysis Laboratory of the Microscopy Centre at Federal University of Minas Gerais (LMA-CM-UFMG).

Standards and quantitative wavelength dispersive X-ray spectroscopy (WDS) analytical parameters were used as described by Chaves et

al. (2013).

To correct the effects of the matrix on the composition and pattern differences, a model proposed by Toya et al. (1984) was applied using ZAF factors. The corrections of X-ray peaks overlapping between Y and Pb were not corrected due to the absence of measurement in PbMa (Lead M alpha), occurring only in PbMb (Lead M beta). The interference of ThMz (Thoruim M gamma) on the measured UMb (Uranium M beta) was correct in order to avoid errors in the obtained ages.

The correction was made as suggested by Chaves et al. (2013), following Scherrer et al. (2000) but adapted to the conditions of the LMA-UFMG, as follows:

$$U_{CORRECTED} = U_{MEASURED} - (0.006365 \times Th_{MEASURED}) \quad (1)$$

The software EPMA Dating (Pommier et al., 2004) was used to calculate the chemical U-Th-P_T ages and associated errors. The average ages were calculated using Isoplot/Ex add-in (Ludwig, 2003). The equation used to age calculation was:

$$Pb = \{Th \times [\exp(\lambda_{232}T) - 1] \times (M_{208}/M_{232})\} + \{U_C \times [\exp(\lambda_{238}T) - 1] \times (M_{206}/M_{238}) \times 0.9928\} + \{U_C \times [\exp(\lambda_{235}T) - 1] \times (M_{207}/M_{235}) \times 0.0072\} \quad (2)$$

Where U_C (U corrected), Th and Pb are concentrations in ppm; T is age in Ma; M_{206}, M_{207}, M_{208}, M_{208}, M_{238}, M_{232} are, respectively, the atomic of ^{206}Pb, ^{207}Pb, ^{208}Pb, ^{235}U, ^{238}U, ^{232}Th; $\lambda_{232} = 0.49475 \times 10 - 4\ Ma^{-1}$; $\lambda_{238} = 1.55125 \times 10 - 4\ Ma^{-1}$; $\lambda_{235} = 9.8485 \times 10 - 4\ Ma^{-1}$ (Pommier et al., 2004).

RESULTS

Petrography

The samples (Figure 2A and D) of West Água Rasa metagranite present similar mineralogical assemblage, distinguishing only in the mineral percentage and texture.

They have phaneritic texture and have as main minerals quartz, plagioclase, microcline and micas, more biotite than muscovite (around 10%) and present apatite, zircon and opaques as accessory minerals.

Monazite appears only in sample 21A. Samples from sites 18 and 21 (Group A) (Figure 2B and C) are fine to medium grained with more microcline while samples collected from site 19 (Group B) (Figure 2E and F) are coarser grained and present more plagioclase.

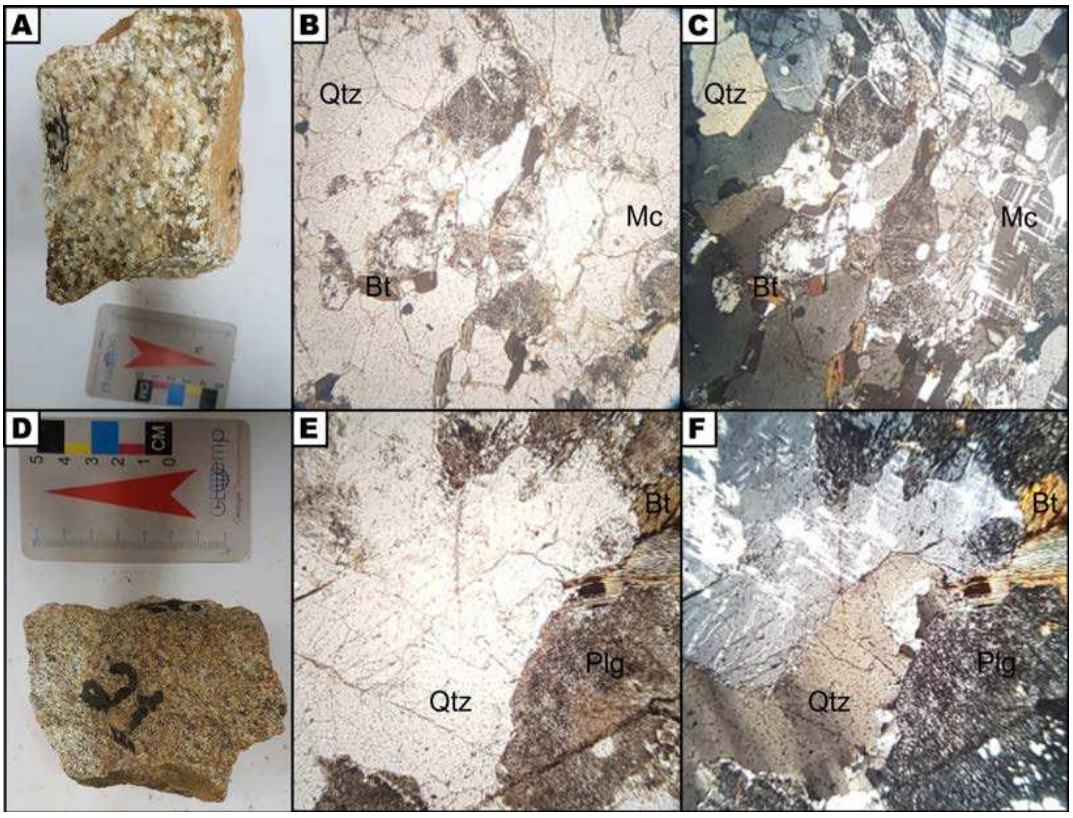

Figure 2 - Hand samples (A, D) and photomicrographies of samples 21 (A, B, C) and 19 (D, E, F) on plane polarized light (B, E) and crossed polarized light (C, F). Mineral abbreviations, in accordance to Whitney & Evans (2010), are: Bt: biotite; Mc: microcline; Plg: plagioclase; Qtz: Quartz.

In the Group A samples, quartz occurs as small to medium grains in which the medium grains are anhedral, fractured, with undulose extinction and the smaller are rounded, some occurring as myrmekite with plagioclase. Microcline occurs in subhedral medium grains with tartan twinning, which some presenting perthitic textures.

Plagioclase also occurs in medium grains; however, they present strong saussurite alteration.

Biotite grains are small, euhedral and slightly oriented, while muscovite is rare and occurs in even smaller elongated grains. In Group B samples all minerals occur coarser, even biotite.

Quartz presents large recrystallized grains with undulose extinction. Plagioclase and microcline are presented in subhedral to euhedral grains, in which few microcline grains may present perthitic texture. Biotite occurs in medium subhedral to euhedral grains and are often altered to chlorite.

Muscovite presents lamellar habit. The modal estimates are in table 1 and the representation of the six samples are plotted in the Streckeisen diagram (Figure 3A) (Streckeisen, 1974), where West Água Rasa metagranite is classified as monzogranite.

Table 1 - Percentage of mineral modal composition of West Água Rasa metagranite samples.

Sample	Mineral modal composition (%)		
	Quartz	Plagioclase	Alkali feldspar
18A	41	25	34
18B	34	28	38
19A	44	33	23
19B	42	38	20
21A	39	28	33
21B	37	26	37

Whole-rock geochemistry

All whole-rock geochemistry data are organized in table 2. West Água Rasa metagranite is classified as granite in TAS diagram (Middlemost, 1994) (Figure 3B) It is a peraluminous (Maniar & Piccoli, 1989) (Figure 3C) leucogranite also plotted in the field of calc-alkalic rocks (Frost et al., 2001) (Figure 3D). In Whalen et al. (1987) diagrams for anorogenic granites, the samples were plotted of the edge of the fields of A-type and I and S-types (Figure 3E and F), while based in Chappell & White (2001) they were classified as S-type (Figure 3G).

Table 2 - Whole rock composition of West Água Rasa metagranite samples.

Sample	Major Elements											
	SiO_2	TiO_2	Al_2O_3	Fe_2O_3	MnO	MgO	CaO	Na_2O	K_2O	P_2O_5	LOI	Total
Detection Limit (%)	0.01	0.01	0.01	0.01	0.01	0.01	0.01	0.01	0.01	0.01	-45	
18A	72.48	0.29	13.28	2.92	0.03	1.18	0.31	2.96	4.27	0.09	1.71	99.52
18B	73.96	0.19	13.07	1.92	0.02	0.66	0.3	2.64	5.14	0.06	1.08	99.04
19A	76.83	0.06	13.43	1.25	0.02	0.16	0.54	2.25	5.34	0.01	1.08	100.97
19B	77.35	0.09	12.59	1.58	0.02	0.19	0.63	2.36	5.19	0.06	0.89	100.95
21A	74.68	0.23	13.31	2.23	0.03	0.32	0.92	3.09	4.6	0.08	0.66	100.15
21B	75.24	0.21	13.24	2.26	0.03	0.3	0.79	2.83	4.72	0.04	1.17	100.83

Sample	Trace Elements											
	Rb	Ba	Sr	Zr	Nb	Y	Ni	Co	Hf	Ta	Th	U
Detection Limit (PPM)	**0.02**	**10**	**10**	**10**	**0.05**	**0.05**	**5**	**0.5**	**0.05**	**0.05**	**0.01**	**0.05**
18A	113.5	838	113	277	8.74	6.88	2	7.3	6.45	0.38	25.9	2.89
18B	138.4	980	125	170	7.2	4.77	2	4.9	4.75	0.48	21.1	2.49
19A	171.8	1068	155	19	4.31	6.12	2	1.6	0.35	0.58	9.5	3.42
19B	153.6	914	149	46	4.36	7.15	2	1.8	1.4	0.56	8	4.77
21A	216.9	592	119	181	13.29	22.13	2	2.7	5.24	0.83	33.6	10.89
21B	223.2	642	113	186	14.89	23.54	2	2.7	5.1	0.99	30.7	8.94

Sample	Rare Earth Elements													
	La	Ce	Pr	Nd	Sm	Eu	Gd	Tb	Dy	Ho	Er	Tm	Yb	Lu
Detection Limit (PPM)	**0.1**	**0.1**	**0.05**	**0.1**	**0.1**	**0.05**	**0.05**	**0.05**	**0.05**	**0.05**	**0.05**	**0.05**	**0.1**	**0.05**
18A	75.9	113.9	14.08	48.5	7.7	1.17	4.87	0.48	2.36	0.29	0.88	0.1	0.6	0.08
18B	52.1	74.8	9.45	32.8	5.4	1.06	3.59	0.36	1.7	0.24	0.61	0.07	0.5	0.06
19A	7.2	12.9	1.2	5.2	1.3	0.66	1.15	0.19	1.31	0.27	0.87	0.11	0.9	0.11
19B	5.7	8.9	0.97	4.3	1.1	0.67	1.15	0.18	1.38	0.27	0.98	0.14	1	0.14
21A	47.2	95.3	10.51	40.4	8.3	0.68	6.41	0.9	5.18	0.9	2.64	0.32	2.2	0.29
21B	44	92.5	9.9	38.2	7.8	0.7	6.15	0.87	5.66	0.9	2.84	0.32	2.6	0.32

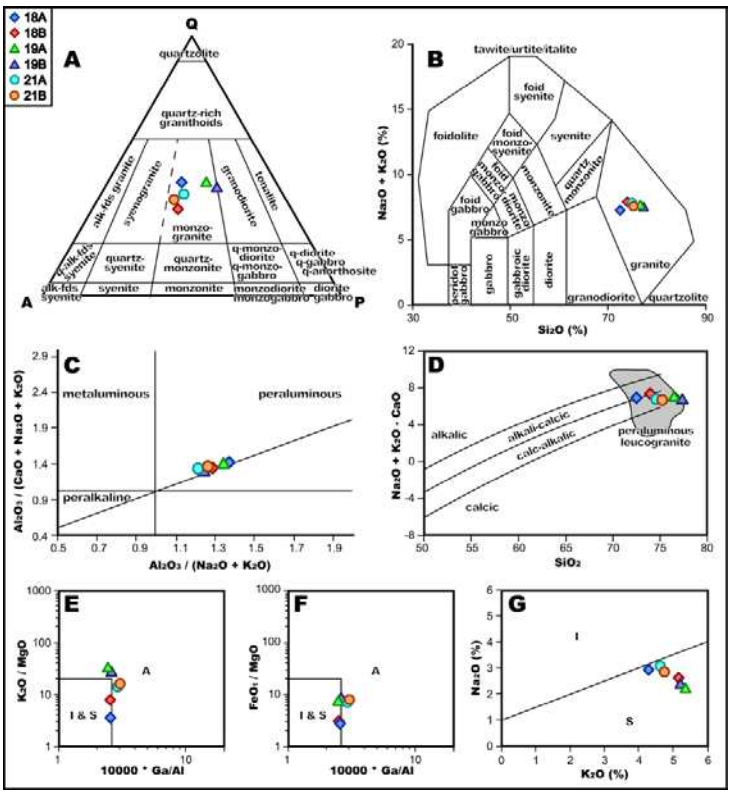

Figure 3 - Lithochemical data from West Água Rasa metagranite plotted on classification diagrams. (A) QAP modal diagram from Streckeisen (1974). (B) Total Alkalis versus Silica (TAS – Middlemost, 1994). (C) Diagram A/CNK- A/NK (Maniar & Piccoli, 1989). (D) Na2O + K2O + CaO vs. SiO2 (wt%) from Frost et al. (2001). (E and F) Anorogenic granite classification diagrams (Whalen et al., 1987). (G) Division between I and S-type of granites (Chappell & White, 2001).

The chondrite-normalized REE patterns (Sun & McDonough, 1989) presented enrichment in light rare earth elements (LREE) and Eu anomaly, positive in samples 19A and 19B, and negative in samples 21A and 21B and slightly negative in samples 18A and 18B (Figure 4A). In the multi-elemental variation diagram normalized to chondrite (Sun & McDonough, 1989) the same Eu behavior is observed. Furthermore, samples 18A, 18B, 21A and 21B showed negative anomalies of Sr, while the opposite is observed in samples 20A and 20B (Figure 4B).

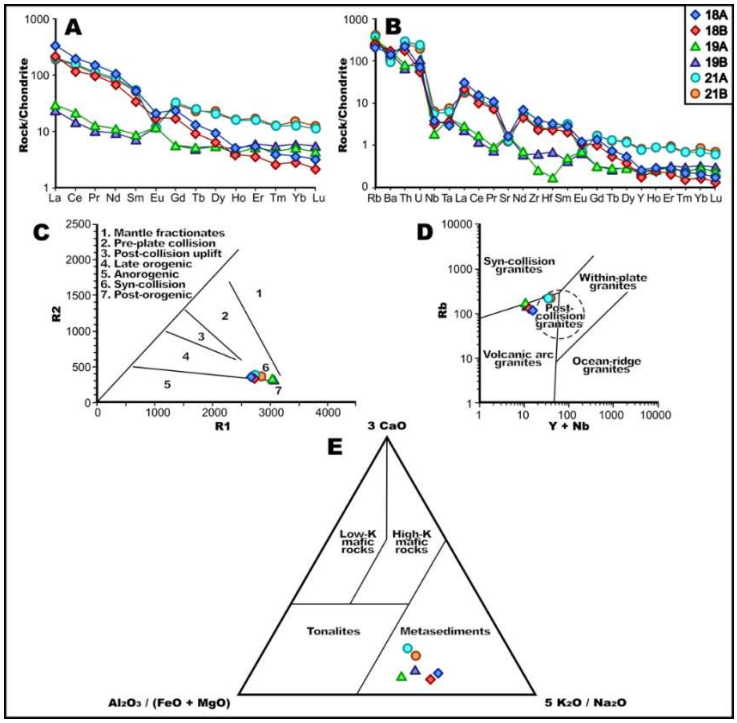

Figure 4 - (A) Chondrite-normalized REE patterns from Sun & McDonough (1989). (B) Multi-elemental spider diagram normalized to N-MORB from Sun & McDonough (1989). (C) R1-R2 diagram (Batchelor & Bowden, 1985). (D) Rb vs. Y+ Nb tectonic diagram from Pearce (1996). (E) Ternary diagram proposed by Laurent et al. 2014).

All samples plotted between syn-collisional to post-orogenic fields in Batchelor & Bowden (1985) diagram (Figure 4C). In Pearce (1996) tectonic diagram (Figure 4D), samples 18A, 18B, 19A and 19B plotted on the edge between syn-collisional to volcanic arc granites, while samples 21A and B plotted on the post-collision granites field. Finally, accordantly to the ternary diagram (Figure 4E) from Laurent et al. (2014), all samples are granites derived from metasediments.

Monazite U-Th-Pb$_T$ geochronology

Monazite grains from sample 21A (West Água Rasa metagranite) are subhedral, very fractured and they show corroded aspect. Backscattered-Electron imaging don't show significative zoning (Figure 5). According to the chemical data (Table 3), the grains are classified as monazite-(Ce).

Three grains (21-mon-01, 21-mon-02 and 21-mon-03) were analyzed with 9 to 10 spots each. Each grain presented half the spots with Statherian age and the others yield Orosirian age (Table 4). The grain 21-mon-01 revealed mean ages of 1778 ± 22 Ma (95% conf., MSWD = 0.53; probability = 0.71) and 1946 ± 27 Ma (95% conf., MSWD = 1.00; probability = 0.39).

The mean ages found in grain 21-mon-02 were 1789 ± 20 Ma (95% conf., MSWD = 0.69; probability = 0.60) and 1871 ± 36 Ma (95% conf., MSWD = 1.2; probability = 0.29). The last grain, 21-mon-03, yield mean ages of 1784 ± 19 Ma (95% conf., MSWD = 0.097; probability = 0.98) and 1904 ± 19 (95% conf., MSWD = 0.12; probability = 0.97) (Figure 5).

The mean Statherian and Orosirian ages found for all grains are, respectively, 1784±20 and 1907±27 Ma.

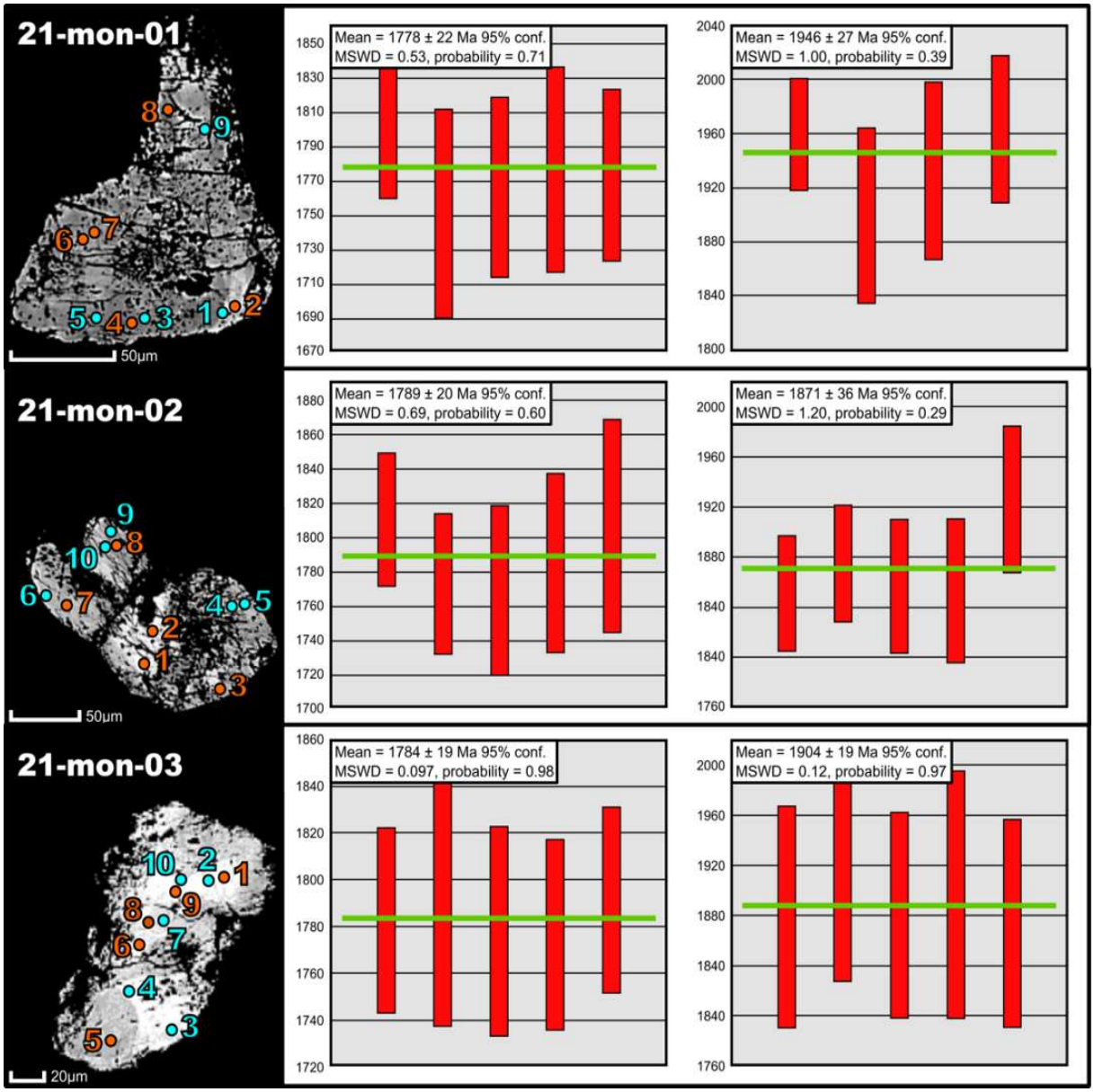

Figure 5 - Backscattered-Electron imaging of monazite grains from sample 21 with respective mean Statherian and Orosirian ages.

Table 3 - Monazite from sample 21 (West Água Rasa metagranite) chemical data.
West Água Rasa monazite from sample 21

21-mon-01															
	P2O5	**SiO2**	**ThO2**	**UO2**	**Y2O3**	**La2O3**	**Ce2O3**	**Pr2O3**	**Nd2O3**	**Sm2O3**	**Gd2O3**	**Dy2O3**	**CaO**	**PbO**	**Total**
1	24.7	3.264	13.5	0.574	2.865	10.86	25.64	2.511	9.497	2.318	1.526	0.904	0.714	1.325	100.2
2	24.84	2.957	12.14	0.563	2.974	12.54	25.35	2.511	9.512	2.407	1.614	0.709	0.818	1.1	100
3	27.04	1.363	5.495	0.286	2.367	13.87	31.58	2.929	10.35	2.139	1.393	0.494	0.481	0.538	100.3
4	27.9	1.524	5.593	0.332	2.489	14.11	29.93	2.998	10.18	2.271	1.455	0.607	0.481	0.513	100.4
5	25.6	1.295	5.45	0.288	2.461	14.41	31.15	2.917	10.4	2.247	1.46	0.461	0.503	0.545	99.19
6	26.89	1.961	7.356	0.338	2.036	11.56	31.06	2.941	10.42	2.014	1.328	0.618	0.487	0.653	99.65
7	26.05	1.572	6.036	0.294	2.294	13.27	31.5	2.924	10.58	2.142	1.484	0.701	0.502	0.544	99.89
8	27.8	1.308	7.231	0.469	2.653	10.27	30.18	2.719	10.27	2.204	1.586	0.699	0.87	0.684	98.94
9	28.48	2.092	7.4	0.312	2.99	9.007	29.36	2.669	10.48	2.303	1.62	0.827	0.641	0.727	98.91

Table 3 – Part 2

21-mon-02															
	P2O5	**SiO2**	**ThO2**	**UO2**	**Y2O3**	**La2O3**	**Ce2O3**	**Pr2O3**	**Nd2O3**	**Sm2O3**	**Gd2O3**	**Dy2O3**	**CaO**	**PbO**	**Total**
1	26.48	3.433	14.12	0.559	2.784	7.95	25.18	2.485	9.55	2.212	1.625	0.693	0.81	1.261	99.15
2	25.64	2.673	10.97	0.471	2.413	10.88	27.77	2.65	9.636	2.338	1.412	0.705	0.782	0.969	99.31
3	27.72	1.917	7.849	0.384	2.288	11.6	30.09	3.011	10.23	1.895	1.416	0.55	0.607	0.705	100.3
4	26.35	2.306	9.087	0.43	2.324	11.84	29.68	2.807	9.938	2.174	1.414	0.674	0.562	0.853	100.4
5	26.11	2.424	9.187	0.415	2.429	11.48	28.96	2.703	10.18	2.175	1.364	0.616	0.582	0.868	99.5
6	26.36	1.872	7.457	0.34	2.132	12.77	31.65	2.826	10.2	1.905	1.365	0.465	0.512	0.669	100.5
7	27.9	1.922	7.629	0.317	2.01	11.92	30.81	2.858	10.23	2.079	1.304	0.652	0.478	0.705	100.8
8	28.07	1.242	6.429	0.367	2.488	12.85	30.78	2.84	10.3	2.065	1.523	0.621	0.664	0.623	100.9
9	28.84	1.334	5.847	0.286	2.354	11.18	31.4	2.837	10.41	2.206	1.428	0.65	0.603	0.537	99.92
10	28.72	1.302	6.522	0.341	2.372	11.61	31.12	2.864	10.2	1.89	1.387	0.627	0.719	0.649	100.3

Table 3 – Part 3

21-mon-03															
	P2O5	**SiO2**	**ThO2**	**UO2**	**Y2O3**	**La2O3**	**Ce2O3**	**Pr2O3**	**Nd2O3**	**Sm2O3**	**Gd2O3**	**Dy2O3**	**CaO**	**PbO**	**Total**
1	26.12	2.615	10.85	0.584	2.876	10.26	27.3	2.646	9.744	2.373	1.729	0.845	0.647	0.998	99.58
2	26.25	2.432	9.788	0.48	2.662	12.96	27.69	2.494	9.554	2.325	1.626	0.812	0.665	0.949	100.7
3	25.32	2.755	11.49	0.528	2.928	11.77	26.42	2.482	9.898	2.279	1.642	0.926	0.699	1.113	100.3
4	25.13	3.023	11.48	0.517	2.563	11.3	26.54	2.676	9.645	2.236	1.5	0.646	0.729	1.099	99.07
5	28.74	1.407	7.115	0.404	2.508	11.22	29.96	2.729	9.901	2.186	1.372	0.746	0.726	0.663	99.68
6	27.35	2.23	9.436	0.389	2.5	11.15	28.13	2.642	10.08	2.116	1.691	0.644	0.633	0.831	99.82
7	26.39	2.18	8.715	0.406	2.597	11.48	29.11	2.905	10.01	2.239	1.611	0.704	0.546	0.842	99.73
8	25.85	2.764	10.89	0.458	2.485	11.91	27.78	2.559	9.66	2.396	1.584	0.585	0.735	0.961	100.6
9	27.27	2.763	10.85	0.566	2.708	11.59	27.23	2.67	9.776	2.288	1.616	0.584	0.648	0.998	101.6
10	25.59	3.034	10.84	0.542	2.779	10.22	27.31	2.717	10.04	2.167	1.693	0.824	0.661	1.053	99.46

Table 4 - Data from sample 21 from West Água Rasa metagranite. Monazite U-Th-Pb_T ages, U, Th and Pb contents and respective errors. MPb is the average Pb atomic mass.

West Água Rasa monazite from sample 21

21-mon-01									
	Age	**Error**	**U**	**Error**	**Th**	**Error**	**Pb**	**Error**	**M Pb**
	Ma	**Ma**	**ppm**	**%**	**ppm**	**%**	**ppm**	**%**	**ppm**
1	1960	42	4305	2.3	118620	1.0	12300	1.0	207.7
2	1798	39	4284	2.3	106669	1.0	10211	1.0	207.7
3	1900	65	2214	4.5	48290	1.0	4994	2.0	207.7
4	1750	61	2614	3.8	49151	1.0	4762	2.1	207.7
5	1933	66	2234	4.5	47895	1.0	5059	2.0	207.7
6	1766	52	2568	3.9	64645	1.0	6062	1.6	207.7
7	1776	60	2254	4.4	53044	1.0	5050	2.0	207.7
8	1773	50	3730	2.7	63546	1.0	6350	1.6	207.6
9	1964	55	2336	4.3	65031	1.0	6749	1.5	207.8

21-mon-02									
	Age	**Error**	**U**	**Error**	**Th**	**Error**	**Pb**	**Error**	**M Pb**
	Ma	**Ma**	**ppm**	**%**	**ppm**	**%**	**ppm**	**%**	**ppm**
1	1810	39	4138	2.4	124104	1.0	11706	1.0	207.8
2	1773	41	3538	2.8	96440	1.0	8995	1.1	207.8
3	1770	50	2946	3.4	68977	1.0	6545	1.5	207.7
4	1853	46	3282	3.0	79857	1.0	7918	1.3	207.7
5	1876	47	3144	3.2	80735	1.0	8058	1.2	207.7
6	1785	52	2580	3.9	65532	1.0	6210	1.6	207.7
7	1858	53	2368	4.2	67044	1.0	6545	1.5	207.8
8	1854	57	2875	3.5	56498	1.0	5783	1.7	207.7
9	1807	62	2194	4.6	51383	1.0	4985	2.0	207.7
10	1927	58	2641	3.8	57315	1.0	6025	1.7	207.7

21-mon-03									
	Age	**Error**	**U**	**Error**	**Th**	**Error**	**Pb**	**Error**	**M Pb**
	Ma	**Ma**	**ppm**	**%**	**ppm**	**%**	**ppm**	**%**	**ppm**
1	1783	40	4541	2.2	95385	1.0	9264	1.1	207.7
2	1900	44	3684	2.7	86017	1.0	8810	1.1	207.7
3	1915	41	4012	2.5	100992	1.0	10332	1.0	207.7
4	1900	41	3915	2.6	100869	1.0	10202	1.0	207.7
5	1790	52	3163	3.2	62527	1.0	6155	1.6	207.7
6	1778	45	2901	3.4	82924	1.0	7714	1.3	207.8
7	1907	48	3091	3.2	76587	1.0	7816	1.3	207.7
8	1777	41	3428	2.9	95736	1.0	8921	1.1	207.8
9	1792	40	4382	2.3	95385	1.0	9264	1.1	207.7
10	1897	42	4171	2.4	95271	1.0	9775	1.0	207.7

DISCUSSION

To characterize the West Água Rasa metagranite were correlated petrographic analyses and whole rock geochemical data from samples 18A, 18B, 19A, 19B, 21A, and 21B.

Then the outcomes were associated with U-Th-Pb_T geochronology results of three monazite grains from sample 21A. The geochemical results, combined with the petrography, were used to classify the rock, its protolith, and genesis.

With the geochemical data, it was possible to correlate the genesis with events already discussed in previous studies (Chaves & Rezende, 2019; Miranda et al., 2020).

From the texture and mineral assemblage observed in thin sections (Figure 2 and Figure 3), associated with TAS classification (Middlemost, 1994) (Figure 3B), it was possible to confirm that the samples are metamonzogranites.

The geochemical data classified the rock with peraluminous nature (Figure 3B and C) and as S-type granite (Figure 3E, F, and G), both indicating supracrustal origin. Moreover, the results indicated that the rock has metasedimentary origin (Figure 4E), confirming that the protolith was formed on an oceanic basin, followed by anatexis of khondalitic graphite-rich rocks and banded iron formations.

The granite genesis is associated to syn- to

post-collisional events (Figure 4C and D). The anomalies of Eu and Sr (Figure 4A and B) are related to the process of metasediments anatexis. They present different anomalies in samples 18A, 18B, 21A, and 21B (negative) and in samples 19A and 19B (positive) due to the predominance of plagioclase in the second group.

The higher concentration of plagioclases in these samples can be explained either by the predominance of minerals rich in Ca in the metasediments that form the metagranites or as a product of a more advanced phase of the anatexis process.

The geochronological data yielded two groups of ages, as shown in Table 5. The Orosirian age is consistent with ages found by Miranda et al. (2020) in Água Rasa metagranites.

Table 5 - Monazite U-Th-Pb$_T$ mean ages from sample 21, West Água Rasa metagranite.

Grain	Age (Ma)	
	Orosirian	**Statherian**
21-mon-01	1946 ± 27	1778 ± 22
21-mon-02	1871 ± 36	1789 ± 20
21-mon-03	1904 ± 19	1784 ± 19

Their results revealed ages of 2077 ± 24 Ma and 1941 ± 23 from monazite and 1934 ± 74 Ma from zircon U-Pb. They characterize the younger ages (~1940 Ma), that are concordant to the results from West Água Rasa metagranites, to the orogen collapse after post-peak decompressional stage, which are coherent to the geochemical results found in samples 21A and 21B (Figure 4B).

The Statherian ages can be correlated with Avanavero-Xiong'er LIP (Figure 6A and 6B), in which the Pará de Minas dyke swarm that crosses the entire area of study (Figure 1A), is part (Chaves, 2021). This hydrothermal process, that occurred around 1.78 ~ 1.79 Ga, was responsible for a regional warming that affected the West Água Rasa metagranites, preserving this event in the monazite. The grains show corroded appearance (Figure 5), typical of hydrothermal dissolution processes, which corroborates this analysis.

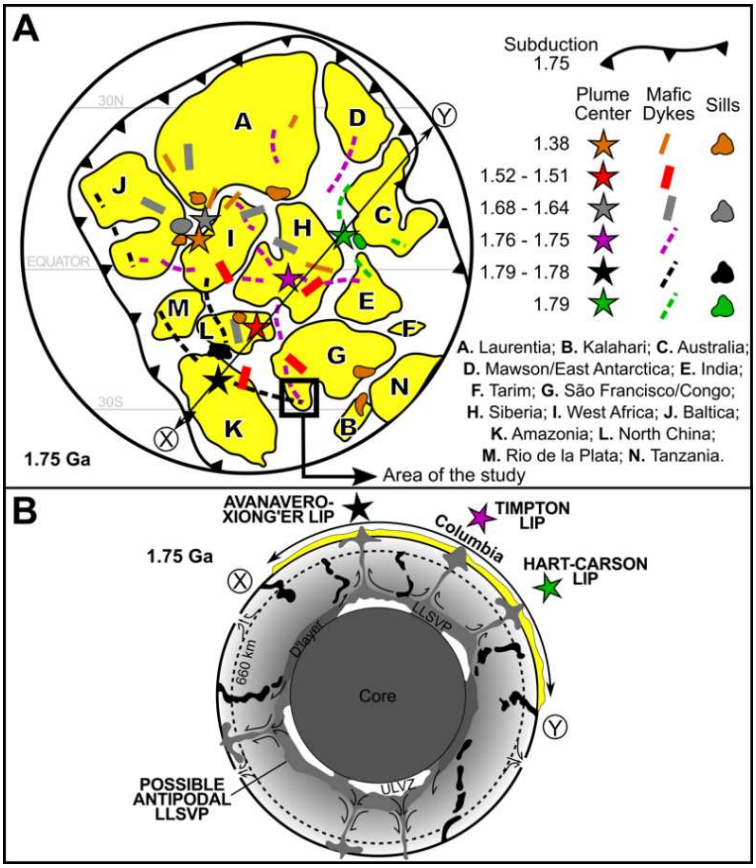

Figure 6 - (A) 1.75 Ga Columbia (Nuna) reconstruction model derived from matching Paleo- to Mesoproterozoic LIP fragments on different cratonic pieces. Radiating dyke systems (and associated volcanics and sills) of not only 1.79 Ga, 1.79–1.78 Ga, and 1.76–1.75 Ga, but also 1.64–1.68 Ga, 1.51–1.52 Ga, and 1.38 Ga LIPs restored on the Columbia (Nuna) are shown with their respective possible plume centers. (B) Supercontinent-superplume coupling suggested for Columbia (Nuna). LLSVP = large low shear velocity provinces, ULVZ = ultra-low velocity zones, SUPERPLUME = cluster of mantle plumes starting from a LLSVP. Modified from Chaves (2021).

The tectonic model in which West Água Rasa metagranites were included is part of a huge collisional orogenic process concentrically developed along all Columbia (Nuna), as shown in Figure 7 (Chaves, 2021). The black square shows the location of the investigated Formiga Paleoproterozoic tectonic processes in figure 7.

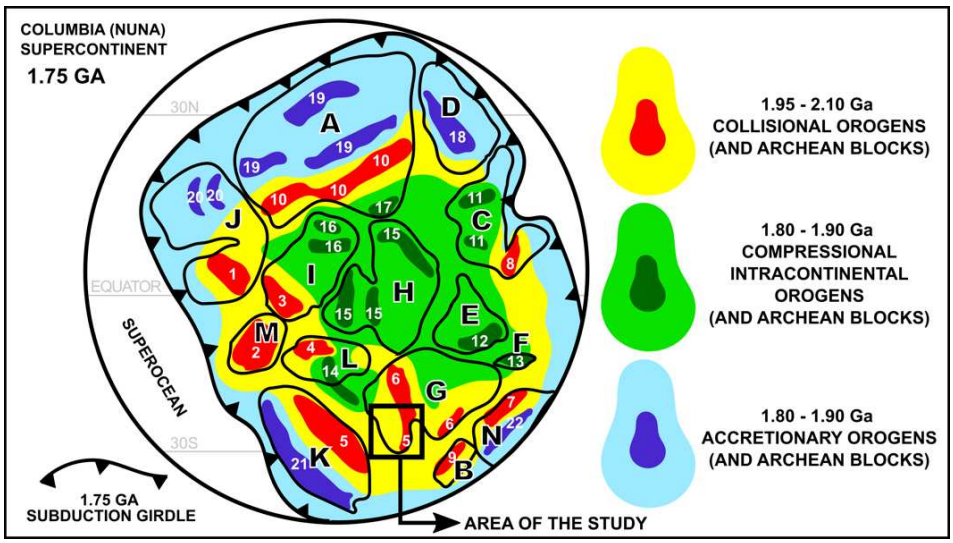

Figure 7 - Distribution of concentric collisional (1.95–2.10 Ga), accretionary and compressional intracontinental (1.80–1.90 Ga) orogens and undiscriminating Archean blocks on 1.75 Ga Columbia (Nuna) reconstruction. Modified from Chaves (2021). A – Laurentia; B – Kalahari; C – Australia; D – Mawson/East Antarctica; E – India; F – Tarim; G – São Francisco/Congo; H – Siberia; I – West Africa; J – Baltica; K - Amazonia; L – North China; M – Rio de La Plata; N – Tanzania; 1 – Volga-Don/Baltica; 2 – Tandilia-Piedra Alta/Rio de la Plata; 3 – Birimian/West Africa; 4 – Khondalite Belt/North China; 5 – Transamazonian/Amazonia and São Francisco craton; 6 – Eburnean and Luizian/Congo craton; 7 – Usagaran/Tanzania; 8 – Glenburg/West Australia; 9 – Limpopo/Kalahari; 10 – Taltson-Thelon and Inglefield/Laurentia; 11 – Mount Isa and Halls Creek/North Australia; 12 – Lesser Himalaya/India; 13 – Tarim/Tarim; 14 – Transnorth China/ North China; 15 – Angara, Akitkan, and Sutam/Siberia; 16 – Zenaga and Reguibat/West Africa; 17 – Wopmay/Laurentia; 18 – Nimrod-Ross/East Antarctica; 19 – Trans Hudson, Torngat-Quebec, and Nagssugtoqidian/Laurentia; 20 – Lapland and Svecofennian/Baltica; 21 – Rio Negro-Juruena/Amazonia; 22 – Ubendian/Tanzania.

CONCLUSION

The West Água Rasa metagranite was formed from the anatexis of supracrustal succession rocks. The melting process of khondalitic graphite-rich rocks and banded iron formations occurred due to the decompression-related orogenic collapse of the Rhyacian-Orosirian event that occurred around 1.90 Ga. A regional warming, associated with the Avanavero-Xiong'er LIP, which is represented in the area by the Pará de Minas dyke swarm, happened between 1.78 and 1.79 Ga and affected the West Água Rasa metagranite. The influence is evidenced by the corroded appearance of monazite grains that presented Statherian age.

ACKNOWLEDGEMENTS

The first author acknowledges the Coordenação de Aperfeiçoamento de Pessoal de Nível Superior - Brasil (CAPES) for the research grant. The second author thanks the support of the Conselho Nacional de Desenvolvimento Científico e Tecnológico (CNPq).

REFERENCES

ALKMIM, F.F. & MARTINS-NETO, M.A. A Bacia Intracratônica do São Francisco: Arcabouço estrutural e cenários evolutivos. In: Martins-Neto M.A., Pinto C.P. (Eds.). **Bacia do São Francisco**. Belo Horizonte: SBG-MG, p. 9-30, 2001.

ASHWORTH, J.R. **Migmatites.** Blackie and Son, Glasgow, p. 302, 1985.

ÁVILA, C.A.; TEIXEIRA, W.; BONGIOLO, E.M.; DUSSIN, I.A.; VIEIRA, T.A.T.; Rhyacian evolution of subvolcanic and metasedimentary rocks of the southern segment of the Mineiro belt, São Francisco Craton, Brazil. **Precambrian Research**, v. 243, p. 221-251, 2014.

BALTAZAR, O.F. & ZUCCHETTI, M. Lithofacies associations and structural evolution of the Archean Rio das Velhas greenstone belt, Quadrilátero Ferrífero, Brazil: A review of the setting of gold deposits. **Ore Geology Reviews**, v. 32, p. 471-499, 2007.

BATCHELOR, R.A. & BOWDEN, P. Petrogenetic interpretation of granitoid rock series using multicationic parameters. **Chemical Geology**, v. 48, p. 43-55, 1985.

BROWN, M. & SOLAR, G.S. Granite ascent and emplacement during contractional deformation in convergent orogens. **Journal of Structural Geology**, v. 20, p. 1365-1393, 1998.

CARNEIRO, M.A. & BARBOSA, M.S.C. Implicações geológicas e tectônicas da interpretação magnetométrica da região de Oliveira, Minas Gerais: **Revista Brasileira de Geofísica**, v. 26, p. 87–98, 2008.

CARVALHO, B.B.; JANASI, V.A.; SAWYER, E.W. Evidence for Paleoproterozoic anatexis and crustal reworking of Archean crust in the São Francisco Craton, Brazil: a dating and isotopic study of the Kinawa migmatite. **Precambrian Research**, v. 291, p. 98-118, 2017.

CHAVES, A.O. Enxames de diques máficos de Minas Gerais – O estado da arte: **Geonomos**, v. 21, p. 29–33, 2013.

CHAVES, A.O.; OLIVEIRA, E.K.; GARCIA, L.R.A. Desenvolvimento do método de datação química U-Th-Pb de monazita por microssonda eletrônica na UFMG: **Geonomos**, v. 21, p. 13–18, 2013.

CHAVES A.O.; CAMPELLO M.S.; PEDROSA-SOARES A.C. Idade U-Th-PbT de monazitas do sillimanita-cordierita-granada-biotita gnaisse de Itapecerica (MG) e a atuação da orogenia Riaciano-Orosiriana no interior do Cráton São Francisco Meridional. **Geociências**, v. 34, p. 324-334, 2015.

CHAVES, A.O. & REZENDE, C.R. Fragments of 1.79-1.75 Ga Large Igneous Provinces in reconstructing Columbia (Nuna): A Statherian supercontinent-superplume coupling?, **Episodes**, v. 24, p. 55–67, 2019.

CHAVES, A.O. Columbia (Nuna) supercontinent with external subduction girdle and concentric accretionary, collisional and intracontinental orogens permeated by large igneous provinces and rifts. **Precambrian Research**, v. 352, p. 106017, 2021.

CHAVES, A.O. & PORCHER, C.C. Petrology, geochemistry and Sm-Nd systematics of the Paleoproterozoic Itaguara retroeclogite from São Francisco/Congo Craton: one of the oldest records of the modern-style plate tectonics. **Gondwana Research**, v. 87, p. 224-237, 2020.

CHAPPELL, B.W. & WHITE, A.J. Two contrasting granite types: 25 years later. **Australian Journal of Earth Sciences**, v. 48, p. 489-499, 2001.

CPRM/CODEMIG. Estado de Minas Gerais-**Mapa Geológico e Mapa de Recursos Minerais em Sistema de Informação Geográfica/SIG. Escala 1: 1000000.** Serviço Geológico do Brasil/CPRM e Companhia de Desenvolvimento Econômico de Minas Gerais/ CODEMIG. DVD Rom, 2014.

DORR, J.V.N. Physiographic, stratigraphic and structural development of the Quadrilatero Ferrifero, Minas Gerais, Brazil, U.S. **Geological Survey Professional Paper**, v. 641, p. 110, 1969.

DRUMMOND, J.B.; PUFAHL, P.K.; PORTO, C.G.; CARVALHO, M. Neoproterozoic peritidal phosphorite from the Sete Lagoas Formation (Brazil) and the Precambrian phosphorus cycle. **Sedimentology**, v. 62, p. 1978-2008, 2015.

EDMONDS, M. & GILL, R. Igneous Rocks and Processes: A Practical Guide. **Geological Magazine**, v. 147, p. 990, 2010.

FARINA F.A.; ALBERT C.; LANA C. The Neoarchean transition between medium and high-K granitoids: Clues from the Southern São Francisco Craton (Brazil). **Precambrian Research**, v. 266, p. 375-394, 2015.

FERNANDES, R.A. & CARNEIRO, M.A.O. Complexo Metamórfico Campo Belo (Cráton São Francisco Meridional): Unidades litodêmicas e evolução tectônica: **Revista Brasileira de Geociências**, v. 30, p. 671–678, 2000.

FROST, B.R.; BARNES, C.G.; COLLINS, W.J.; ARCULUS, R.J.; ELLIS, D.J.; FROST, C.D. A geochemical classification for granitic rocks. **Journal of petrology**, v. 42, p. 2033-2048, 2001.

HARRIS, N.; VANCE, D.; AYRES, M. From sediment to granite: timescales of anatexis in the upper crust. **Chemical Geology**, v. 162, p. 155-167, 2000.

LAURENT, O.; MARTIN, H.; MOYEN, J.F.; DOUCELANCE, R. The diversity and evolution of late-Archean granitoids: Evidence for the onset of "modern-style" plate tectonics between 3.0 and 2.5 Ga. **Lithos**, v. 205, p. 208-235, 2014.

LUDWIG, K.R. Isoplot/Ex 3.00: **A geochronological toolkit for Microsoft Excel:** Berkeley Geochronology Center, Special Publication, v. 4, p. 70, 2003.

MACHADO, N.; SCHRANK, A.; NOCE, C.M.; GAUTHIER, G. Ages of detrital zircon from Archean-Paleproterozoic sequences: Implications for greenstone belt setting and evolution of a Transamazonian foreland basin in Quadrilátero Ferrífero, southeast Brazil: Evidence from zircon ages by laser ablation ICP-MS. **Earth Planetary Science Letters**, v. 141, p. 259-276, 1996.

MACHADO FILHO, L.; RIBEIRO, M.; GONZALES, S.R.; SCHENINI, C.A.; SANTOS NETO, A.; PALMEIRA, R.C.; PIRES, J.L.; TEIXEIRA, W.; CASTRO, H.E.F. **Geologia das folhas Rio de Janeiro (SF 23/24) escala 1:1.000.000, mapa e texto explicativo.** Rio de Janeiro: RADAM Brasil, Ministério das Minas e Energia, p. 780, 1983.

MANIAR, P.D. & PICCOLI, P.M. Tectonic discriminations of granitoids. **Geological Socitey of America Bulletin**, v. 101, p. 635–643, 1989.

MIDDLEMOST, E.A.K. Naming materials in magma/igneous rock system. **Earth-Science Reviews**, v. 37, p. 215–224, 1994.

MIRANDA, D.A.; CHAVES, A.D.O.; DUSSIN, I.A.; PORCHER, C.C. Paleoproterozoic khondalites in Brazil: a case study of metamorphism and anatexis in khondalites from Itapecerica supracrustal succession of the southern São Francisco Craton. **International Geology Review**, p. 1-25, 2020.

MOREIRA, H.; LANA, C.; NALINI JÚNIOR, H.A. The detrital zircon record of an Archaean convergent basin in the Southern São Francisco Craton, Brazil. **Precambrian Research**, v. 275, p. 84-99, 2016.

NOCE, C.M.; MACHADO, N.; TEIXEIRA, W. U-Pb Geochronology of gneisses and granitoids in the Quadrilatero Ferrıfero (Southern São Francisco Craton): Age constraints for Archean and Paleoproterozoic magmatism and metamorphism. **Revista Brasileira de Geociências**, v. 28, p. 95-102, 1998.

NOCE, C.M.; PEDROSA-SOARES, A.C.; SILVA, L.C.D.; ALKMIM, F.F. O embasamento arqueano e paleoproterozóico do orógeno Araçuaí. Geonomos, v. 15, p. 17-23, 2007.

PEARCE, J. Sources and settings of granitic rocks. **Episodes**, v. 19, p. 120-125, 1996.

POMMIER, A.; COCHERIE, A.; LEGENDRE, O. EPMA Dating User's manual: Age calculation from electron probe microanalyser measurements of U-Th-Pb. BRGM Documents, p. 9, 2004.

READ, H. H. Meditations on granite: part one. **Proceedings of the Geologists' Association**, v. 54, p. 64-85, 1943.

SCHERRER, N.C.; ENG, M.; GNOS, E.; JAKOB, V.; LIECHTI, A. Monazite analysis; from sample preparation to microprobe age dating and REE quantification. **Schweizer Mineralogische und Petrographische Mitteilungen**, v. 80, p. 93-105, 2000.

STRECKEISEN, A.L. Classification and Nomenclature of Plutonic Rocks: Recommendations of the IUGS Subcommission on the Systematics of Igneous Rocks. **Geologische Rundschau. Internationale Zeitschrift für Geologie. Stuttgart**, v. 63, p. 773–786, 1974.

SUN, S.S. & MCDONOUGH, W.F. Chemical and isotopic systematics of oceanic basalts, implications for mantle composition and processes, in Saunders, A.D., Norry, M.J., eds., **Magmatism in the ocean basins**, v. 42: London, Geological Society of London, p. 313–345, 1989.

TEIXEIRA, W.; CARNEIRO, M.A.; NOCE, C.M.; MACHADO, N.; SATO, K.; TAYLOR, P.N. Pb, Sr and Nd isotope constraints on the Archean evolution of gneissic-granitoid complexes in the southern São Francisco Craton, Brazil. **Precambrian Research**, v. 78, p. 151-164, 1996.

TEIXEIRA, W.; ÁVILA, C.A.; DUSSIN, I.A.; CORRÊA NETO, A.V.; BONGIOLO, E.M.; SANTOS, J.O.S.; BARBOSA, N. A juvenile accretion episode (2.36–2.33 Ga) in the Mineiro belt and its role to the long-lived Minas accretionary orogeny: zircon U–Pb–Hf and geochemical evidences. **Precambrian Research**, v. 256, p. 148-169, 2015.

TEIXEIRA, W.; OLIVEIRA, E.P.; PENG, P.; DANTAS, E.L.; HOLLANDA, M.H.B.M. U-Pb geochronology of the 2.0 Ga Itapecerica graphite-rich supracrustal succession in the São Francisco Craton: Tectonic matches with the North China

Craton and paleogeographic inferences. **Precambrian Research**, v. 293, p. 91-111, 2017.

TOYA, T.; KATO, A.; JOTAKI, R. Quantitative Analysis with Electron Probe Microanalyzer. **Jeol Training Center.** Japan, p. 113, 1984.

WHALEN, J.B.; CURRIE, K.L.; CHAPPELL, B.W. A-type granites: geochemical characteristics, discrimination and petrogenesis. **Contributions to mineralogy and petrology**, v. 95, p. 407-419, 1987.

WHITNEY D.L. & EVANS B.W. Abbreviations for names of rock-forming minerals. **American Mineralogist**, 95,185-187.

ZHOU, J. & LI, X. 2006. **GeoPlot: An excel VBA program for geochemical data plotting**: Computers e Geosciences, v. 32, p. 554–560, 2010.

Submetido em 7 de junho de 2021
Aceito para publicação em 8 de novembro de 2021